17TH ADVANCED BEAM DYNAMICS WORKSHOP ON
FUTURE LIGHT SOURCES

LCLS X-Ray Optics: Design Status and R&D Overview

R. Tatchyn, SSRL/SLAC

APRIL 6-9, 1999
ARGONNE NATIONAL LABORATORY, ARGONNE, IL U.S.A.

LCLS X-Ray Optics: Design Status and R&D Overview*

Roman Tatchyn[a,b]
Stanford Synchrotron Radiation Laboratory, Stanford Linear Accelerator Center, Stanford, CA 94305, USA

TALK OVERVIEW:

- **LCLS source properties (preliminary studies)**
  - coherent
  - spontaneous
  - Bremsstrahlung

- **LCLS X-Ray Optical system (preliminary design)**
  - the absorption cell
  - instrumentation

- **R&D Program (1999-2001)**
  - coherent source properties
  - spontaneous source properties
  - Bremsstrahlung
  - high peak power radiation/matter interactions
  - non-linear effects
  - short-pulse effects
  - instrumentation
    - beam characterization
    - microfocusing
    -

- **CDR**

---

* This work was supported in part by the Department of Energy Offices of Basic Energy Sciences and High Energy and Nuclear Physics, and Department of Energy Contract DE–AC03–76SF00515.
[a] for the LCLS X-Ray Optics Design Study Group:J. Arthur, R. Boyce, A. Fasso, J. Montgomery, V. Vylet, D. Walz, Andreas K. Freund, Malcolm Howells.
[a]Corresponding author: Email: tatchyn@ssrl01.slac.stanford.edu; TEL: 650-926-2731; FAX: 650-926-4100

- **LCLS source properties (preliminary studies)**

Table 1. Optical and physical parameters of the LCLS. Undulator K=3.67. N_u=3300 periods. Undulator period λ_u=3 cm.

Radiation wavelength [Å]	1.5	15
Norm. emitt. $\gamma\varepsilon$ [mm-mrad]	1.5	2.0
Electron energy [GeV]	14.35	4.54
Peak current [A]	3400	3400
Bunch duration [fs, FWHM]	277	277
Peak spontaneous power [GW]	81	4.9
Peak coherent power* [GW]	9	11
Average coherent power** [W]	0.31	0.35
Energy/pulse [mJ]	2.5	0.64
Coherent photons/pulse ($x10^{12}$)	1.9	23
Approx. Bandwidth (BW) [%]	0.1	0.1
Peak brightness*** ($x10^{32}$)	12	1.48
Peak degeneracy parameter [$x10^9$]	3.3	412
Average brightness*** ($x10^{21}$)	40	4.9
Transverse size [μm, FWHM]****	78	93
Divergence angle [μrad, FWHM]****	1	8
Spontaneous fundamental opening angle [μrad, FWHM]	4.9	15.5
Spontaneous fundamental transverse size [μm, FWHM]	82	131
Peak Power Density [W/mm^2]** ($x10^{12}$)**	**1.88**	**1.62**
Peak Field [V/m]**($x10^{10}$)**	**3.8**	**3.5**
*Output fully transversely coherent; **at 120 Hz pulse rep rate; ***Photons/s/mm^2/mrad^2/0.1%BW; ****At undulator exit		

- **LCLS brightness & degeneracy parameter:**

$$B = \frac{N_{phot}/\sigma_\tau}{(2\pi)^3 \varepsilon_x \varepsilon_y \left(\frac{\sigma_f}{f}\right)}$$

$$\delta = \frac{(\lambda/2)^2 N_{phot}}{(2\pi)^3 \varepsilon_x \varepsilon_y \sigma_\tau \sigma_f} = B\left(\frac{\lambda^3}{4c}\right),$$

- **source brightness**

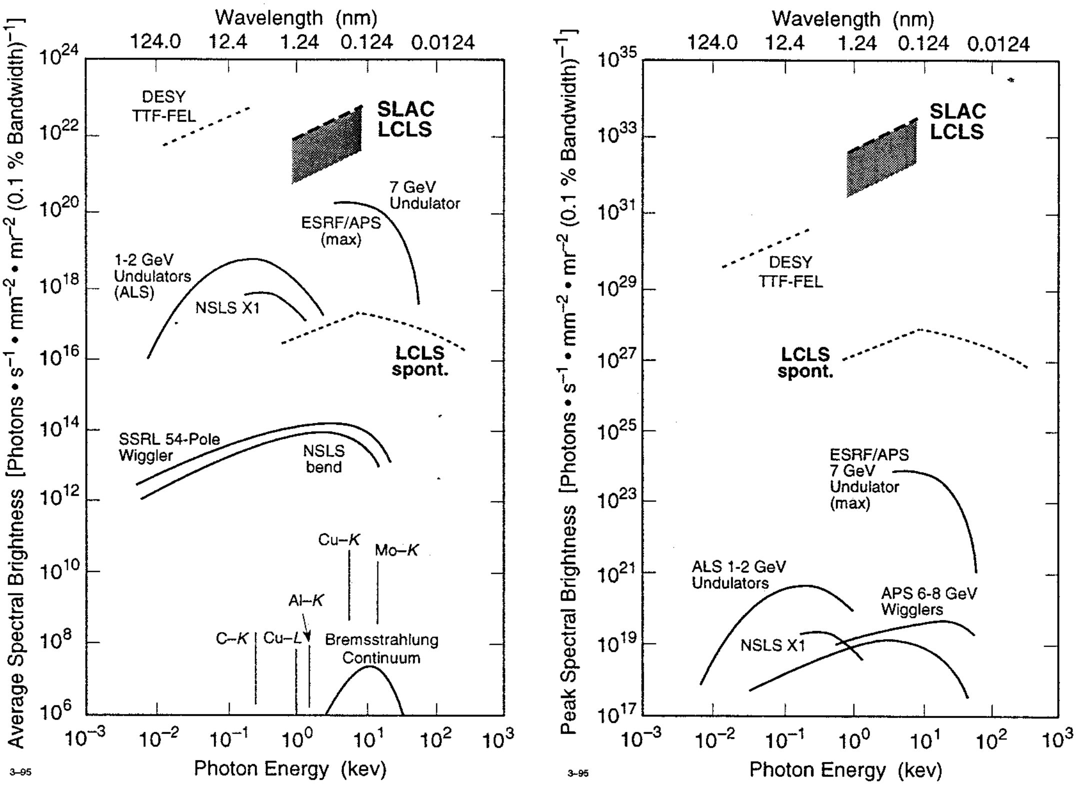

Figure 3.1.2. Comparative peak and average brightness curves contrasting the LCLS with alternative quasi-coherent sources.

- **temporal structure**

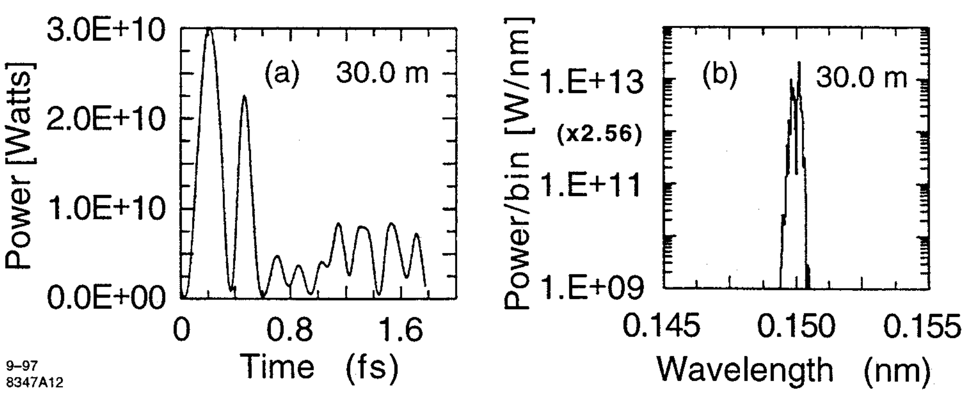

Figure 3.1.1. Temporal (a))and spectral (b)) features of the saturated output of a 30 m 1.5 Å SASE FEL. The abscissa of b) is divided into 256 bins.

- **spontaneous radiation:**

  - **assumptions:**

    - far field
    - 0 emittance
    - 0 energy spread

  - **justification:**

    - obtain conservative power density estimates
    - can factor in emittance effects analytically

  - **target geometry:**

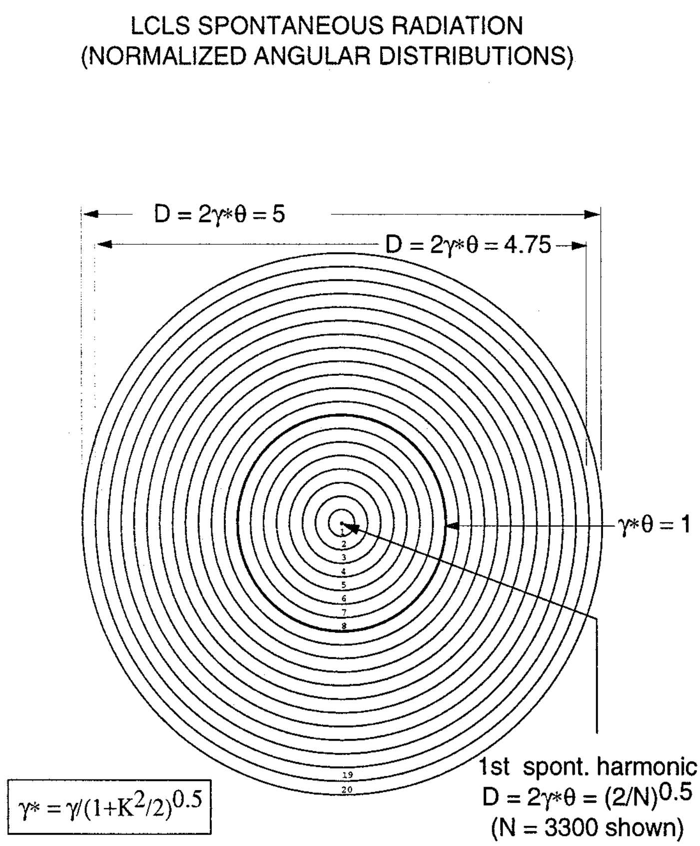

Figure 3.2.1.1. Far-field radial target geometry for the spontaneous radiation emitted by the LCLS undulator.

- **spontaneous radiation:**

- **far-field spectra:**

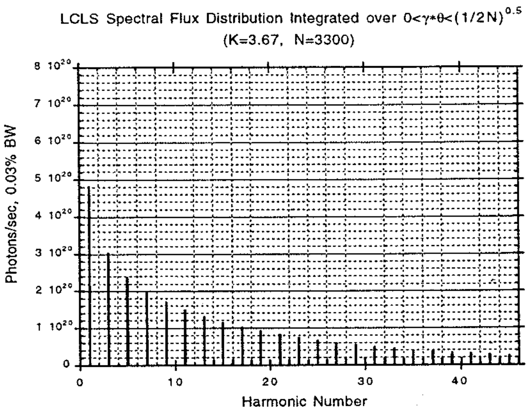

Figure 3.2.1.2. LCLS spontaneous flux distribution integrated over the FWHM aperture of the fundamental.

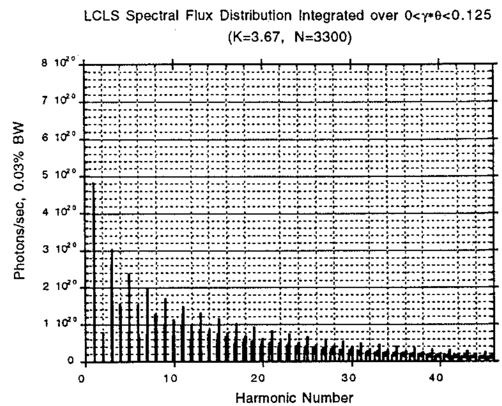

Figure 3.2.1.3. Spontaneous LCLS flux distribution integrated over a small aperture near the axis.

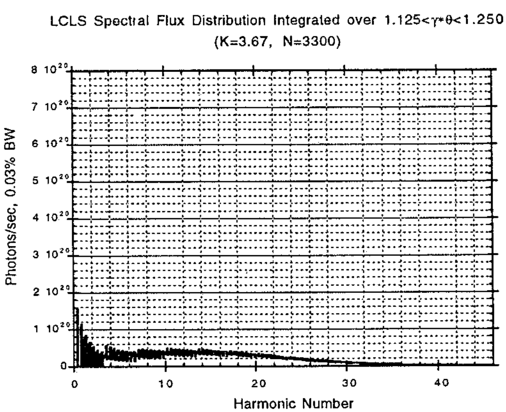

Figure 3.2.1.4. Spontaneous LCLS flux distribution in a narrow annular region away from the axes.

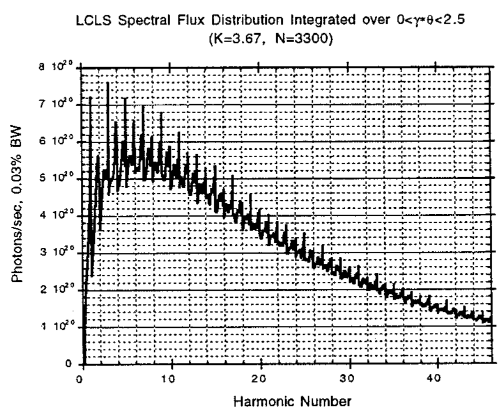

Figure 3.2.1.5. Spontaneous LCLS flux distribution integrated over a large finite aperture.

Paper Presented at the 1997 SPIE Annual Meeting, August 1, 1997, San Diego, CA; ms. #3154-22

• SPONTANEOUS/COHERENT POWER DENSITiES

Spontaneous Power and Power Density Distributions vs. γ*θ for the SLAC LCLS
(Distance = 10 meters, K=3.67)

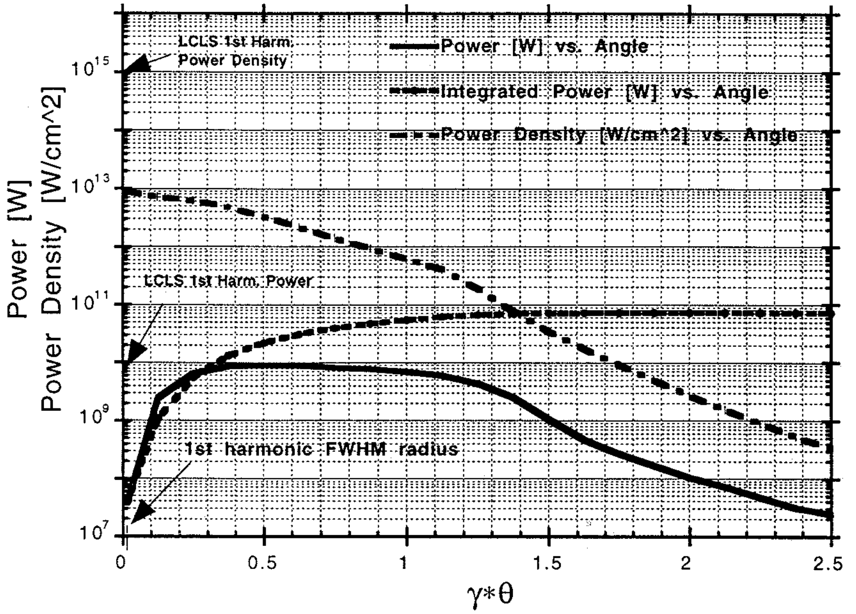

Spontaneous Power and Power Density Distributions vs. γ*θ for the SLAC LCLS
(Distance = 10 meters, K=3.67)

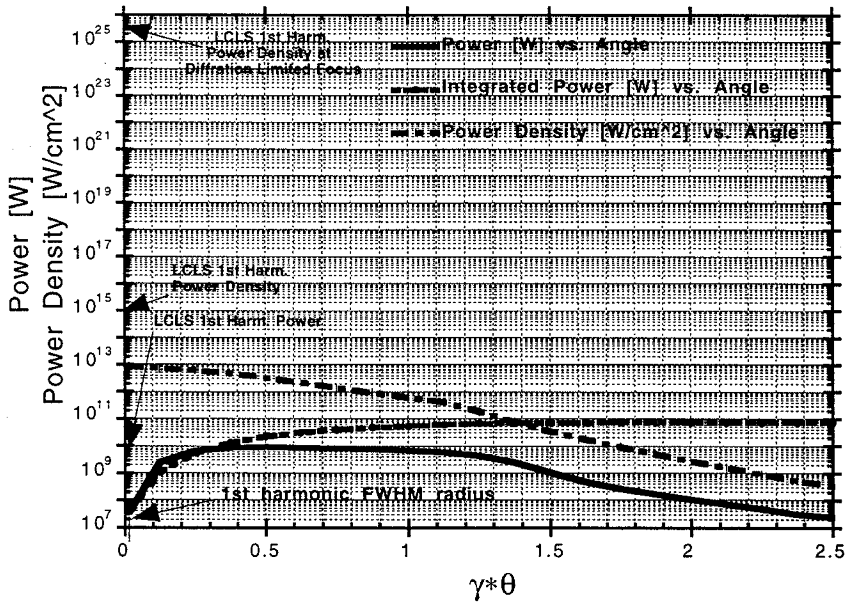

- **Bremsstrahlung**

LCLS vs. storage ring average bremsstrahlung (coarse estimate):

	LCLS	Storage Ring	LCLS/SR
Straight (und):	100m x 1μT	2m x 1nT	$5x10^4$
Straight (collim. equiv.)	300m x 1μT	N/A	$\underline{1.5x10^5}$
			$2x10^5$
Current (av.)	0.15 μA	100mA	$3.75x10^{-7}$
Energy	15 GeV	3 GeV	5

Ratios in LCLS/SR column multiply out to ~0.2 (cannot disregrad!)

STATUS:

- **Bremsstrahlung cone has 1/γ angle (>> coherent FEL angle).**
- **assume 0.1% beam-bremsstrahlung conversion (=> 50 GW!) and 10% transmission into experimental area**
- **with absorption cell, bremsstrahlung power >> coherent FEL power**
- **10^{11} duty factor implies concern for detector response**
- **bremsstrahlung fluxes have been calculated and experimental areas have been designed to suppress neutron noise**
- **more comprehensive simulations will be continued**

- **schematized LCLS X-Ray Optical system**

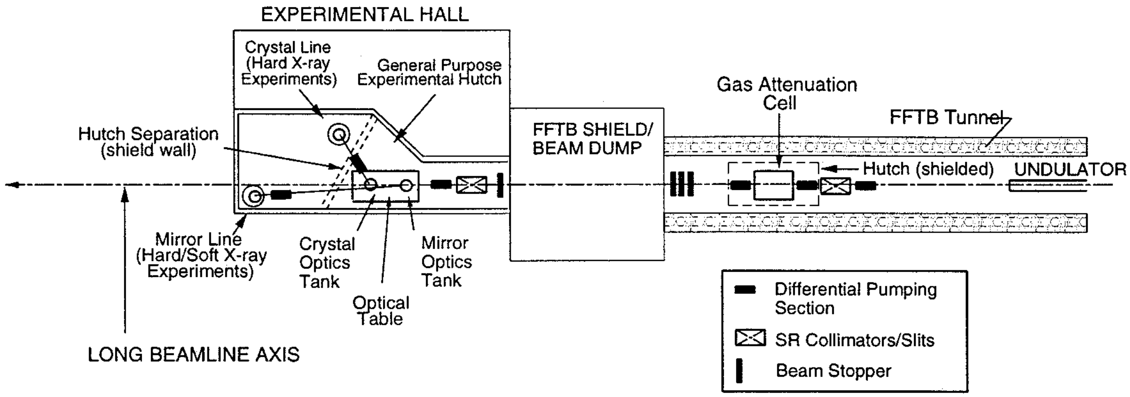

- **preliminary design**

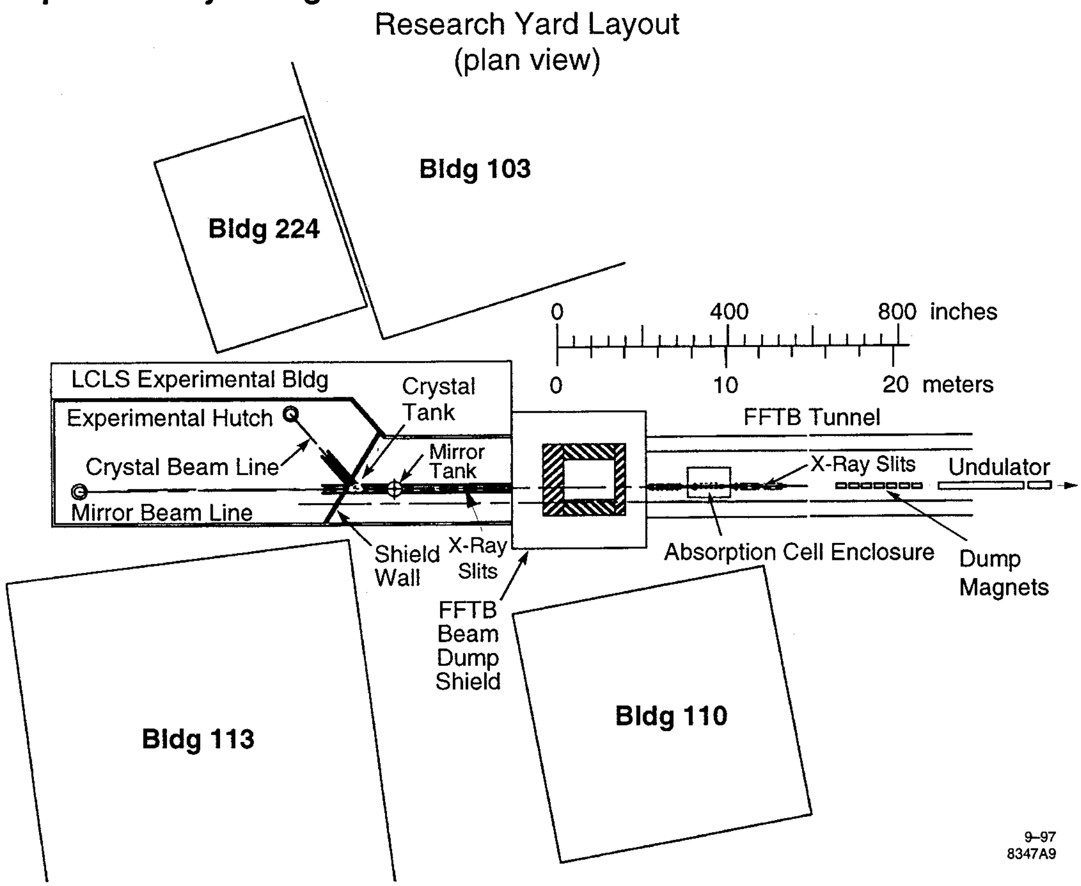

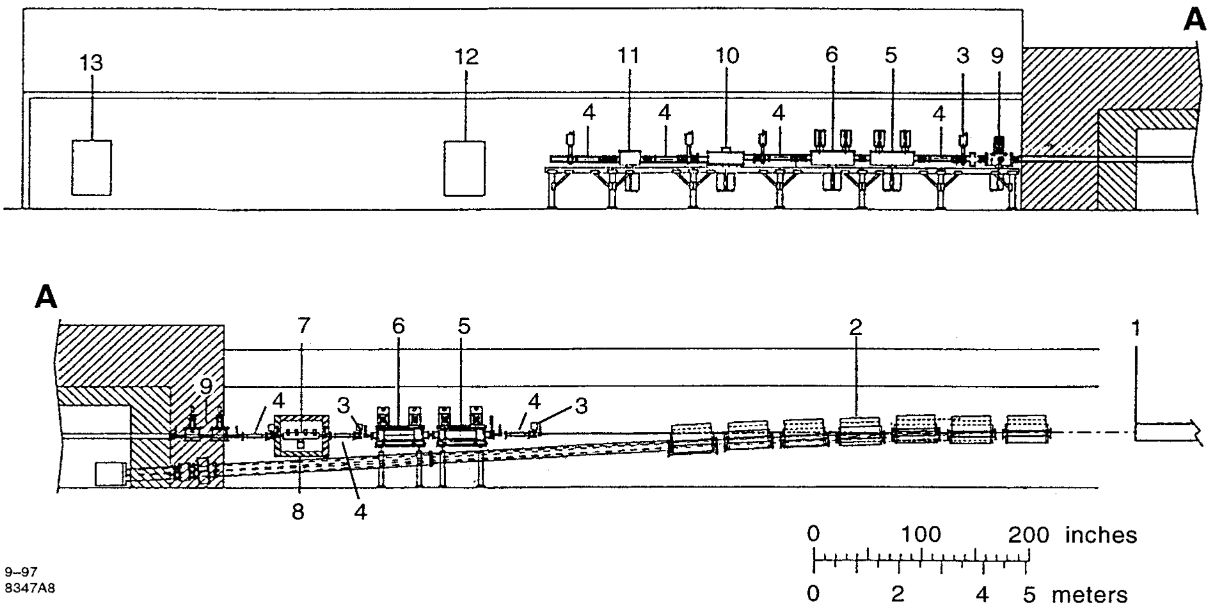

Figure 2.1.2. Detailed layout (elevation view) of electron beam dump line and the X-ray optics system components in the LCLS undulator-to-experimental-area. 1-undulator exit; 2-electron beam dump magnets; 3-vacuum valve; 4-Differential Pumping Section (DPS); 5-vertical X-ray slits; 6-horizontal X-ray slits; 7-absorption cell; 8-absorption cell radiation enclosure; 9-beam shutter; 10-mirror tank; 11-crystal tank; 12-crystal beam line end station; 13-specular beam line end station.

- **the absorption cell**

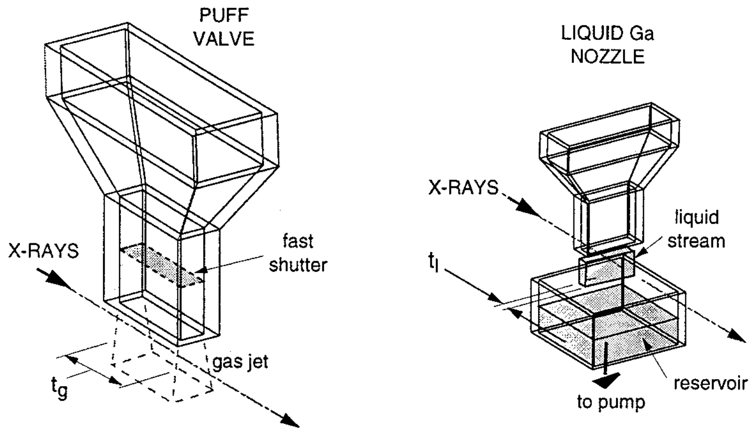

Figure 4.1.4.1. Schematized gas (left) and liquid (right) nozzle configurations for the LCLS absorption cell.

Table 4.1.4.1. Absorption cell valve and vacuum parameters. Valve orifice width 250 µm; t_g=1cm; gas jet height 1 mm.

Valve Rep Rate [Hz]	120	12
Valve Pressure [Torr]	7500	7500
Particles/Puff	6.65×10^{17}	6.65×10^{17}
Chamber Pump Capacity [l/s]	1800	1800
Gas Load Q [Torr-l/s]	2.25	0.225
Average Pressure [Torr]	1.25×10^{-3}	1.25×10^{-4}

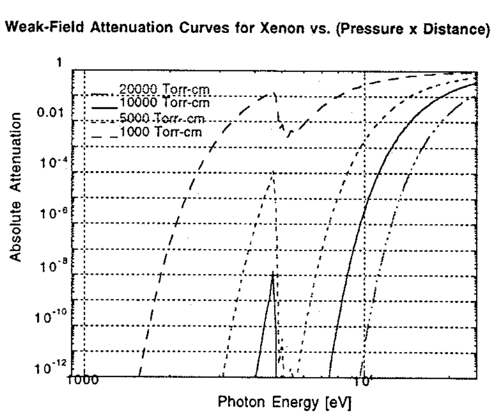

Figure 4.1.4.2. Weak-field attenuation curves for xenon.

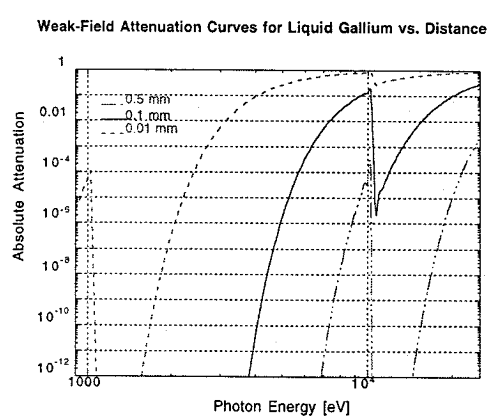

Figure 4.1.4.3. Weak-field attenuation curves for gallium.

- **instrumentation (cold matter, weak-field optical constants):**
  - **mirrors:**

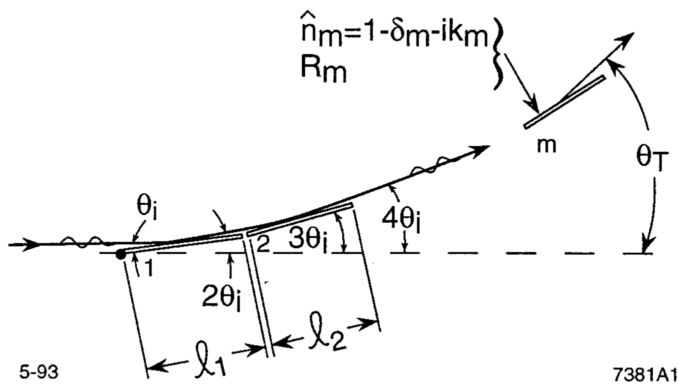

Figure 4.1.5.1. Tandem-grazing-incidence reflector geometry. R_m is the reflectivity and $\hat{n}_m$ the complex index of refraction of the mth reflector.

$$\eta_A\,[\text{eV/atom}] = \frac{P_{peak}\sqrt{2\pi\sigma}\,\tau}{q}\left[\frac{\theta_i}{D_w^2}\right]\left[\frac{1-R}{\delta_p \#}\right].$$

$$R_{TM} = \frac{\rho^2(\sin\theta_i - \rho)^2 + k^2}{\rho^2(\sin\theta_i + \rho)^2 + k^2}\ ; \qquad R_{TE} = R_{TM} \times \frac{\rho^2(\cos\theta_i\cot\theta_i - \rho)^2 + k^2}{\rho^2(\cos\theta_i\cot\theta_i + \rho)^2 + k^2}$$

Here

$$\rho = \{[\sin^2\theta_i - 2\delta + \sqrt{(\sin^2\theta_i - 2\delta)^2 + 4k^2}]/2\}^{1/2}.$$

Note

$$\sin\theta_{ic} \cong \theta_{ic} = (2\delta)^{1/2}$$

implies advantage for higher-Z materials.
However, for $\theta_i \ll \theta_{ic}$,

$$R_{TE(TM)} \cong 1 - 2(k/\delta)\cdot\left(\theta_i / \sqrt{2\delta - \theta_i^2}\right) + \dots\ ,$$

implies advantage for lower-Z materials.

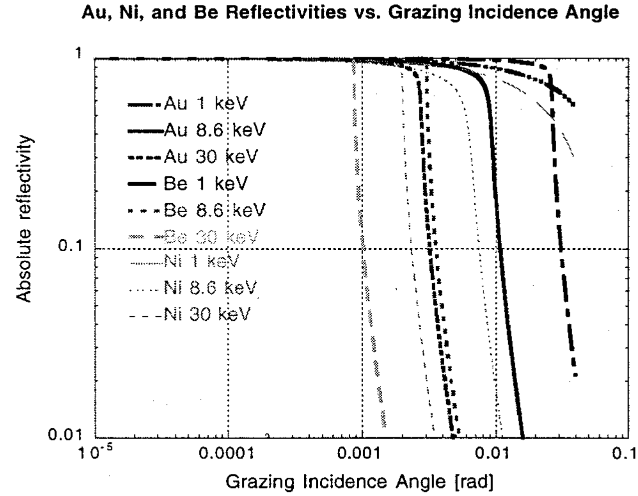

Figure 4.1.5.2. Reflectivity (TE) of candidate LCLS mirror materials vs. grazing incidence angle and LCLS energy.

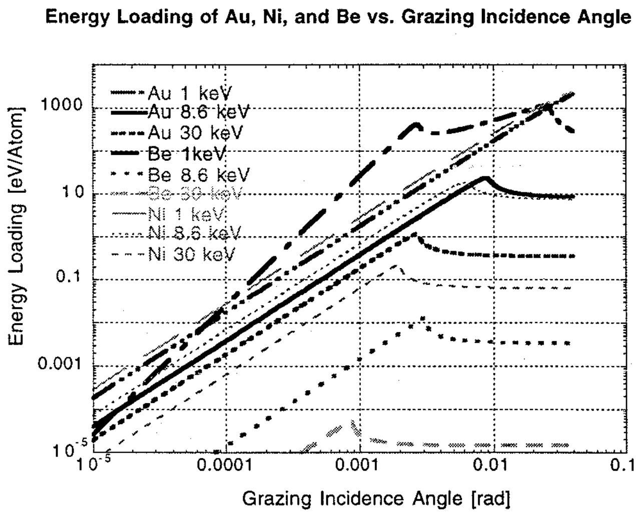

Figure 4.1.5.3. Peak power energy loading of candidate LCLS mirror materials vs. (TE) grazing incidence angle and LCLS energy.

Table 4.1.5.1. LCLS mirror bank parameters. D_W~100 μm.

Mirror Material	Energy Range	m	L [m]	θ_i[rad]	θ_T[rad]	η_A ($x10^{-4}$) [eV/atom]
Beryllium	3-30 keV	1	0.25	0.0004	0.0004	6-0.12
Gold	<3 keV	2	1	0.0001	0.0004	200

- **crystals (A. Freund & ESRF collab. et al):**

Table 4.1.6.1. Comparison of monochromator materials: beryllium, diamond (C*), silicon and germanium..

Material	Be	C*	Si	Ge
Atomic Number (Z)	4	6	14	32
Atomic Weight (A)	9	12	28	73
Crystal Structure	hcp	diamond	diamond	diamond
Lattice Constant a [Å]	2.286	3.567	5.431	5.658
Lattice Constant c [Å]	3.583	-	-	-
a)Debye Temperature T_D [K]	1188	1860	543	290
b)Absorption Coefficient μ [cm^{-1}]	1.8	7.5	1.41	402
a)Conductivity κ [$Wcm^{-1}K^{-1}$]	1.93	23	1.5	0.64
a)Expansion Coefficient α [$10^{-6}K^{-1}$]	7.7	1.1	2.4	5.6
a)$\kappa/\mu\alpha$ [MW]	0.14	2.78	4.4×10^{-3}	2.8×10^{-4}
c)$\kappa/\mu\alpha$ [MW]	11	120	0.20	6.6×10^{3}
a)297 K; b)at 8 keV; c)77 K				

- energy loading estimate

$$\eta_A\,[\text{eV/atom}] \cong \frac{P_{peak}\sqrt{2\pi\sigma_\tau}}{q t_a D_w^2 \#}$$

Table 4.1.6.3. Selected crystal and energy loading parameters under LCLS beam conditions at 1.5 Å. D_W=100 µm. Assumed crystal thickness ~t_e.

Material	Lattice Spacing d_H [Å]	1st Order Diffraction Angle [°]	Resolution [$\Delta\lambda/\lambda$] ($\times10^{-6}$)	η_A [eV/atom]
Be (002)	1.7916	24.1.75	22.8	**0.014**
Be (110)	1.1428	41.02	7.1	**0.009**
C* (111)	2.0593	21.36	59.7	**0.069**
C*(220)	1.2611	36.49	19.3	**0.042**
Si (111)	3.1354	13.84	135	**2.011**
Si(220)	1.9200	22.99	57.7	**1.232**

- **R&D Program (1999-2001):**

- coherent source properties

- phase space properties*

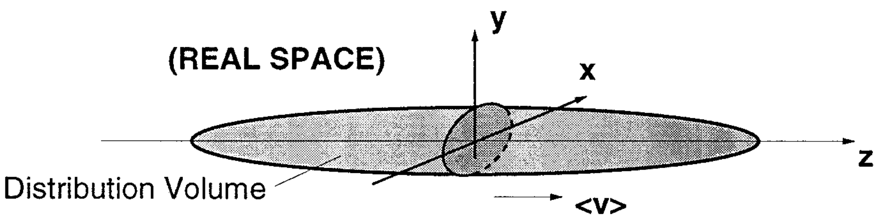

Figure 1. Real subspace of (6-dimensional) phase space. Shaded regions denotes the distribution volume

Table 1. Phase space dimensions, statistical moments, and pdfs.

PHASE SPACE DIMENSION	DISTRIBUTION MEAN	DISTRIBUTION VARIANCE	HIGHER DISTRIBUTION MOMENTS	→	PROBABILITY DENSITY FUNCTION
x	$\langle x\rangle$	$\langle(x-\langle x\rangle)^2\rangle$	• • •	→	?
y	$\langle y\rangle$	$\langle(y-\langle y\rangle)^2\rangle$	• • •	→	?
z	$\langle z\rangle$	$\langle(z-\langle z\rangle)^2\rangle$	• • •	→	?
p_x	$\langle p_x\rangle$	$\langle(p_x-\langle p_x\rangle)^2\rangle$	• • •	→	?
p_y	$\langle p_y\rangle$	$\langle(p_y-\langle p_y\rangle)^2\rangle$	• • •	→	?
p_z	$\langle p_z\rangle$	$\langle(p_z-\langle p_z\rangle)^2\rangle$	• • •	→	?

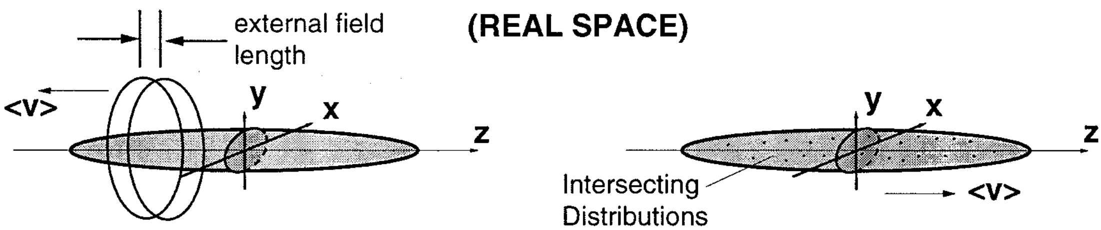

Figure 2. Interacting phase space distributions: interaction (viewed in the electron bunch frame) with an external field shorter than the bunch (left); interaction between two intersecting (e.g., electron and radiation) distributions (right).

*R. Tatchyn and J. Arthur; ms. 3451-26 SPIE98, 7/23-24/98, San Diego, CA

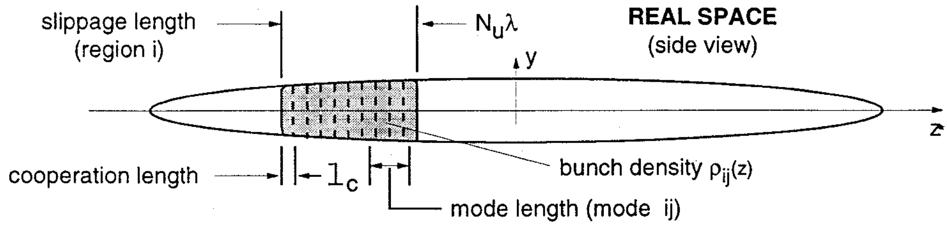

Figure 4 Real-space representation of the mode structure of an ultrarelativistic coherent radiation source.

$$B = \frac{N_{phot}(hf)}{\eta^3 \Delta x \Delta x' \Delta y \Delta y' h \Delta f} = \frac{N_{phot} / \Delta\tau}{\eta^3 \Delta x \Delta x' \Delta y \Delta y' (\Delta f / f)} .$$

Units of **B** [photons/s,mm^2,mr^2,0.1%BW]. For the case of a Gaussian distribution (e.g., storage ring), we associate $\Delta x \rightarrow \sqrt{2\pi/\eta}\,\sigma_x$, $\Delta y \rightarrow \sqrt{2\pi/\eta}\,\sigma_y$, $\Delta x' \rightarrow \sqrt{2\pi/\eta}\,\sigma_{x'}$, $\Delta y' \rightarrow \sqrt{2\pi/\eta}\,\sigma_{y'}$, $\Delta\tau \rightarrow \sqrt{2\pi/\eta}\,\sigma_\tau$, and $\Delta f \rightarrow \sqrt{2\pi/\eta}\,\sigma_f$. In that case,

$$B = \frac{N_{phot} / \sigma_t}{8\pi^3 \sigma_x \sigma_{x'} \sigma_y \sigma_{y'} (\sigma_f / f)} .$$

The associated degeneracy parameter, δ, defined as the number of coherent photons per (unit) mode volume, is given by

$$\delta = \frac{N_{phot}}{\eta^3 \Delta x \Delta x' \Delta y \Delta y' c \Delta\tau (\Delta f / c)} = \frac{(\lambda^3) N_{phot} / \Delta\tau}{\eta^3 c \Delta x \Delta x' \Delta y \Delta y' (\Delta f / f)} = \left(\frac{\lambda^3}{c}\right) B .$$

In numerical terms,

$$\delta = 3.3 \times 10^{-24} (\lambda[A])^3 B .$$

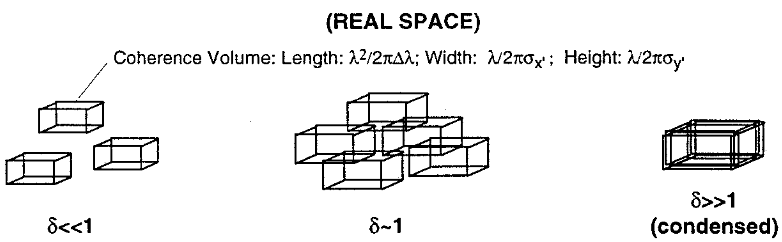

Figure 5. Real space representation of three regimes of the degeneracy parameter δ.

- **realistic phase space description:**

$$B = \frac{< N_{phot(ij)} > / < \Delta\tau_{ij} >}{< \eta_{ij}^{3} >< \Delta x ><_{ij} \Delta x_{ij}' >< \Delta y_{ij} >< \Delta y_{ij}' > (< \Delta f_{ij} > / < f_{ij} >)}$$

- two types of description are of interest:
- (distinction does not arise on storage rings due to CL theorem)

1) "projected" Brightness ("frequency" series)
2) B(z) , Δx(z), Δx'(z), etc. ("time" series)

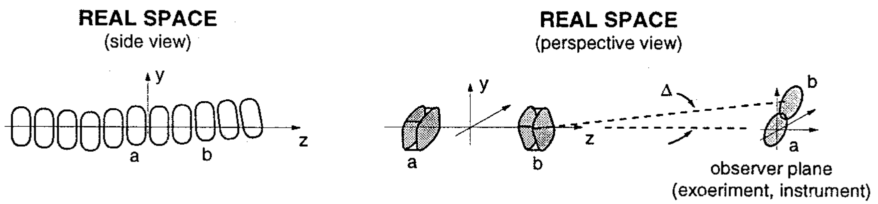

Figure 6 Real space representation of non-constant electron bunch phase space parameters (vs. z). Representations not to scale.

- critical for experimenters and instrumentation designers

- essential for describing coherence transport

OTHER ESSENTIAL R&D ACTIVITIES:

- **spontaneous source properties**
  - near-field calculations
  - spontaneous radiation from bunched distributions (required for harmonics and subharmonics adjacent to theLCLS fundamental)
- **Bremsstrahlung**
  - time-dependent thermal neutron simulations
- **high peak power radiation/matter interactions**
  - theory
  - numerical simulations
  - experimental investigations
- **non-linear effects**
  - theory
  - numerical studies
- **short-pulse effects**
  - theoretical and numerical studies
- **instrumentation development**
  - peak power loading
  - dynamic/disposable optics
  - multi-phase optics
  - extension of LCLS parameter space
- **beam characterization**
  - detectors
  - beam splitters, autocorrelators
- **microfocusing**
  - Snigirev (refractive) lenses; zone plates
- **experimental design**
  - special purpose optics
  - metrology
- **CDR**
  - by 2001-2002